The crust anisotropy of west Ordos block and its geodynamic implications

Jinyu Lv[1], Xuzhang Shen[1], Liuting Huang[1], Xiaohui He[1], He Huang[1], Wenjun Zheng[2], and Dongli Zhang[3]

[1]School of Earth Science and Geological Engineering, Sun Yat-Sen University
[2]Guangdong Provincial Key Laboratory of Geodynamics and Geohazards, School of Earth Sciences and Engineering, Sun Yat-Sen University
[3]Sun Yat-sen University

November 23, 2022

Abstract

Based on the teleseismic records of the dense broadband seismic array, the crustal anisotropy parameters of the west Ordos block and its adjacent regions were determined with P wave receiver functions. The results indicate that the dominant direction of the fast wave is N-S in the Alxa block, NEE-SWW in north Ordos block, N-S in south Ordos block, and E-W in the Yangtze block. The fast wave direction of crust anisotropy in north Ordos block is distinctly different from the south Ordos block and the Alxa block. The Dabashan thrust fold belt is a visible boundary of crust anisotropy, which implies that the crust anisotropy kept the information of ancient South China block and North China block. Comparing with the direction of the fast wave from the SKS splitting, we tentatively discussed the interaction mode between the crust and mantle. The crust and mantle are decoupled in south Ordos block and coupled in north Ordos block. Combining the results of previous geophysical studies, we presented a crust-mantle interaction model to explain the geophysical observations. The most prominent features of the model are the horizontal eastward expansion of the mantle material in the southern Ordos and the vertical upwelling of the mantle material in the northern Ordos. The different modes of movement of the mantle material led to the deep contrasting structures of north and south Ordos, including the crust anisotropy. The mantle upwelling also implies that north Ordos block might be currently experiencing craton destruction.

Posted on 23 Nov 2022 — CC-BY 4.0 — https://doi.org/10.1002/essoar.10504838.1 — This a preprint and has not been peer reviewed. Data may be preliminary.

The crust anisotropy of west Ordos block and its geodynamic implications

Jinyu Lv1,2, Xuzhang Shen1,2*, Liuting Huang 1,2, Xiaohui He1,2, He Huang1,2, Wenjun Zheng1,2, Dongli Zhang1,2

1 Guangdong Provincial Key Lab of Geodynamics and Geohazards,School of Earth Sciences and Engineering, Sun Yat-Sen University,Guangzhou 510275, China

2 Southern Marine Science and Engineering Guangdong Laboratory(Zhuhai),Zhuhai 519082,China

Corresponding author: Xuzhang Shen (shenxzh5@mail.sysu.edu.cn)

Key Points:

- The crust anisotropy has been constrained by the the records of the dense broadband seismic array in the west Ordos block.
- The fast wave direction of crust anisotropy in north Ordos block is distinctly different from the south Ordos block and the Alxa block.
- The contrasting structures beneath north and south Ordos block are controlled by the different movement of mantle material.

Abstract

Based on the teleseismic records of the dense broadband seismic array, the crustal anisotropy parameters of the west Ordos block and its adjacent regions were determined with P wave receiver functions. The results indicate that the dominant direction of the fast wave is N-S in the Alxa block, NEE-SWW in north Ordos block, N-S in south Ordos block, and E-W in the Yangtze block. The fast wave direction of crust anisotropy in north Ordos block is distinctly different from the south Ordos block and the Alxa block. The Dabashan thrust fold belt is a visible boundary of crust anisotropy, which implies that the crust anisotropy kept the information of ancient South China block and North China block. Comparing with the direction of the fast wave from the SKS splitting, we tentatively discussed the interaction mode between the crust and mantle. The crust and mantle are decoupled in south Ordos block and coupled in north Ordos block. Combining the results of previous geophysical studies, we presented a crust-mantle interaction model to explain the geophysical observations. The most prominent features of the model are the horizontal eastward expansion of the mantle material in the southern Ordos and the vertical upwelling of the mantle material in the northern Ordos. The different modes of movement of the mantle material led to the deep contrasting structures of north and south Ordos, including the crust anisotropy. The mantle upwelling also implies that north Ordos block might be currently experiencing craton destruction.

Keywords：crust anisotropy; Ordos block; receiver function; crust-mantle interaction

Plain Language Summary

· The Ordos block was stable without strong tectonic activity and showed rigid movement characteristics, which has been believed as a typical craton. But some of the new results from geophysics showed that the crust of the Ordos block is not a single and a stable structure with an obvious low-velocity layer within the crust, striking high Poisson’s ratio in north Ordos block and a low-velocity anomaly in the mantle in north Ordos, which indicate that the interior of the Ordos is no longer a stable block, as well laid a good foundation to further explore the deep dynamic process of this area. Here, we constrain the crust anisotropy by the the teleseismic records of the dense broadband seismic array in the west Ordos block and its adjacent regions.

The results indicated the contrasting structures beneath north and south Ordos block, which implies the different movement of mantle material.

1.Introduction

The Ordos block is a part of the ancient North China Craton (Ding, 1991). Since the Mesozoic era, due to the subduction of the ancient Pacific, an east-to-west differentiation occurred in the North China Craton. The eastern lithospheric base of the North China Craton is active (Griffin et al., 1998; Deng et al., 2004; Jie , 2001), while the west part is believed to form the stable Ordos block. Being subsequently suffered from the Yanshan movement and the Xishan movement, the Ordos block continued to uplift (Deng et al., 1999). In the south Ordos block, the Qinling-Dabie orogen is the boundary between North China and South China, which experienced a multistage orogenic evolution with accretion and collision between discrete continental blocks. South Qinling, which includes the north Dabashan thrust belt, is located south of the Shangdan suture and was a passive continental margin during the early Palaeozoic era (Li et al., 2014; Dong and Santosh, 2016).

The Ordos block was stable without strong tectonic activity (Jia et al., 2014; Guo et al., 2004; Deng et al., 1999; Li et al., 2002) and showed rigid movement characteristics (Gan et al., 2007). These phenomena show that the Ordos block conforms to the characteristics of the craton's stable crust. In general, a typical craton should be characterized by a stable and archaic continent along with a high-density and low-velocity ratio in crustal structure. With the accumulation of high-density and high-quality broadband digital seismic data, some high-resolution and high-precision imaging of the crust, upper mantle, and even deeper interior structures were obtained. Some of the results, however, showed that the crust of the Ordos block is not a single and a stable structure. For example, results from a wide-angle reflection and refraction indicated an obvious low-velocity layer at 20 km depth in north Ordos block (Jia et al., 2015). Dong et al. (2014) found a low resistivity anomaly in the lithosphere in the southwestern corner of the block with a three-dimensional magnetotelluric (MT) inversion. Based on the observations from a dense broadband seismic array, Wang et al. (2017) obtained the Poisson's ratio with h–κ stacking method showing a striking high Poisson's ratio in north Ordos block.

77 Tomographic images also show a low-velocity anomaly in north Ordos at the upper mantle
78 (Zhang et al., 2018; Guo et al., 2017). These results indicate that the interior of the Ordos is no
79 longer a stable block, as well laid a good foundation to further explore the deep dynamic process
80 of this area.

81 Anisotropy in the crust and mantle indicates a seismological parameter most closely related
82 to the process of geodynamics (Silver, 1996). The direction of the anisotropic fast wave is
83 closely related to the direction of material migration, the orientation arrangement of a crystal
84 lattice, and the deformation history during the tectonic evolution. Therefore, the results of
85 seismic anisotropy might be used to reveal information on the geodynamic process. Shear wave
86 splitting measured on the SKS phase is a classical method to determine the anisoropy occurred
87 on the upward ray path through the mantle between the core-mantle boundary and the surface on
88 the receiver side. However, SKS splitting is nearly always interpreted in terms of upper mantle
89 anisotropy, and a potential contribution from the lower mantle is ignored (Savage, 1999, Long
90 and Silver, 2009). Receiver function is another valid method to measure the crust anisotropy by
91 analzing the arrival time and polarity of P-to-S converted waves caused by the interfaces on
92 radial and tangential components. Many research works have been carried out to constrain the
93 crust and upper most mantle anisotropy with receiver functions (Frederiksen and Bostock, 2010;
94 Long, 2013; Mccormack et al., 2013; Brownlee et al., 2017; Bar et al., 2019).

95 Many scholars have studied the crust and mantle anisotropy in the northeast margin of the
96 Tibetan Plateau and the Ordos block and discussed the deep dynamic process. Yu et al. (2016)
97 analyzed the seismic anisotropy of the southern Ordos block and the Qinling-Dabie orogenic belt
98 on the basis of the SKS wave splitting and proposed that the belt had an eastward mantle
99 material migration channel response to the horizontal expansion of the Tibetan Plateau. Chang et
100 al. (2017) analyzed the anisotropy of the upper mantle in Ordos block with the XKS wave
101 splitting and obtained the direction of the anisotropic fast inside the Ordos block is near N-S
102 direction in the north, and near E-W direction in the south. Huang et al. (2008) discussed the
103 formation mechanism of the anisotropy on the southern edge of the Ordos block using the S-
104 wave splitting method and proposed that the Ordos block had a counterclockwise rotation trend.
105 The previous anisotropic results in the Ordos block are mainly from the XKS (SKS, SKKS, and
106 PKS) splitting and obtained the migration of the upper mantle materials. Shen et al. (2015)

documented a low-velocity anisotropic layer in the lower crust in the northeastern margin of the Tibetan Plateau based on radial and tangential components of a receiver function. These results give important information about the deep dynamic process in the northeast margin of the Tibetan Plateau and the Ordos block; however, the resolution and coverage are still limited due to the small number of observations and uneven distributions.

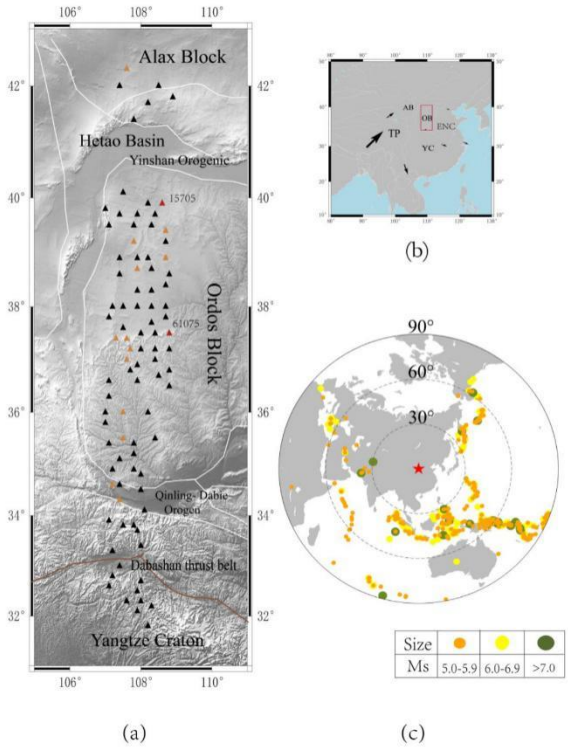

Figure 1. Map of the research area and stations. (a) Distribution of seismic stations. The triangle represents the station position, and white lines are the block boundary. The receiver functions of stations with a red triangle are shown in Figures 2 and 3. The station with a black triangle represents stations with periods rule of π for the PMs arrival in radial receiver functions. The station with a yellow triangle represents a kind of stations with periods rule of 2π for the PMs arrival in radial receiver functions. (b) Other first order blocks around the study area. The red box indicates the location of the study area. The black arrows show the relative movement directions of the active tectonics. (c) Epicenters distribution of earthquake events. The red star is the central location of the study area. The abbreviations are: Tibetan Plateau (TP), Ordos Block (OB), Yangtze Craton(YC),Eastern North China Craton (ENC), Alax Block(AB).

In this paper, the crustal anisotropy parameters are constrained using P wave receiver functions from dense broadband seismic array covering west Ordos block, part of the Alxa block, and the Yangtze block as shown in Figure 1. Referring to the previous seismic results, we discussed the tectonic significance and deep dynamic process of the western Ordos.

2.Observations and Method

During 2013- 2016, the dense broadband seismic array, ChinArray-Himalaya II, was set up with 675 stations in the northeast margin of the Tibetan Plateau by the institute of geophysics of China Earthquake Administration (Wang et al., 2017). In this study, we used the waveforms of teleseismic earthquakes from 92 temporary broadband stations of the ChinArray-Himalaya II in the west Ordos block and its adjacent regions (Figure 1a). Distribution of the stations is a north-south section with a uniform and good coverage from the Yangtze block to the Alxa block across the Ordos block. The massive observations might ensure us to obtain high-quality receiver functions and good constraints of the deep structures.

During the work of the seismic array between September 2013 to June 2016, the teleseismic records of surface-wave magnitude (Ms) ≥ 5.5 with epicenter distances of 30~90° range were selected; the distribution of seismic events is shown in Figure 1c. The original records of the three components (N-E-Z) of the original data were rotated to radial (R), tangential (T), and vertical (Z) components. The three-component records were cut in the time windows of 20s prior to and 120s after the P arrival. Receiver functions were calculated by deconvolving the vertical component from the radial and tangential components, respectively, using an iterative approach (Ligorria and Ammon, 1999). A low-pass Gaussian filter with a half-width constant of 1.0 was applied to regulate the deconvolution. Moveout correction is then applied for a reference slowness of 6.4 s/° to correct the influence of different distances. Furthermore, we constructed binning stacks of R component of receiver functions (RRFs) and T component of receiver functions (TRFs) for each of the stations in an azimuth interval of 6°.

The seismic anisotropy parameters can be represented by the fast direction (FD) and split time (δt) (Crampin & Stuart, 1987; Silver & Chan, 1991). When the P wave passes through the isotropic medium layer, there is no energy on TRFs. In addition, the arrival P-to-S(PMs) conversions on RRFs from the Moho with different back-azimuth is the same. For the anisotropic layered crust, the incoming P wave splits into a fast and a slow component, causing the azimuth-dependent of arrivals of PMs on RRFs and the polarity reversal on the TRFs. The TRF exhibit significant azimuthal variation and polarity reversal. In the previous studies, we used the time variations of the PMs conversions from the Moho in the RRFs and the azimuth-

weighted stacking of TRFs (AWST) to determine the FD and the magnitude of the anisotropy (delay time) and obtained the anisotropic low-velocity layer in the lower crust beneath the northeast margin of the Tibetan Plateau (Shen et al., 2015). Here, the same method was applied to the observations to constrain the anisotropic parameters in the western Ordos block. In the following paragraphs, we present the results of two typical stations to describe the method briefly (Figure 1a).

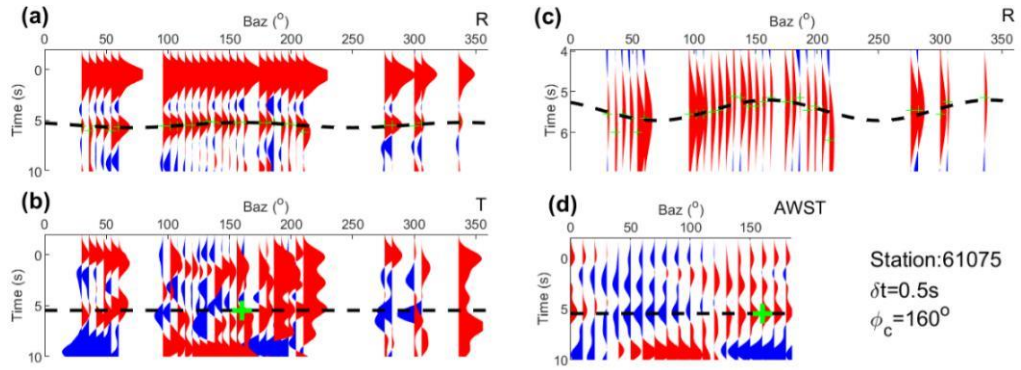

Figure 2. Observed receiver functions and AWST section of station 61075. (a) RRFs. Thin green pluses mark the PMs arrivals. The black dashed line marks the arrival of the PMs phase predicted by the anisotropic model. (b) TRFs. The black-dashed line marks the average value of the PMs arrivals. The green plus marks the location of the azimuth related to the FD of the anisotropic layer determined by the AWST section in Figure 2d. (c) Zoomed-in RRFs in a narrow time window to highlight the variation of the PMs arrivals. The black-dashed line marks the arrival of the PMs phase predicted by the anisotropic model. (d) AWST section. The green plus marks the azimuth of the maximum stacking amplitude from the lower interface, which corresponds to the FD of the anisotropic layer. The black dashed line marks the average value of the PMs arrival. The station name, split time (δt), and FD ($ø_c$) are also marked.

Station 61075 represents a kind of station with π periodicity of arrivals of PMs against back-azimuth, implying a single layer of anisotropy with a horizontal symmetry axis. We selected 158 RRFs and TRFs to construct the binning stacks in a back-azimuth interval of 6° (Figures 2a and 2b). Figure 2c indicates the zoomed time window to highlight the arrival times (green plus signs) of PMs on RRFs (Figure 2a). We obtained the FD and the delay time by fitting the observed arrivals of PMs. In addition, the TRFs show the periodic rule of π around the arrival time of PMS (Figure 2b). A reversal of polarity in the TRFs seems to exist at an azimuth of 160°. However, the pattern is not so clear for the poor coverage. The AWST section in Figure 2d shows a clear pattern of anisotropy. We estimated the FD at 160° azimuth using the maximum

amplitudes (Shen et al., 2015). Finally, the anisotropy parameters of the crust below the station were obtained: the delay time is 0.11s and the FD is 160°. The results of the FD from RRFs and TRFs are consistent, which implies further reliability.

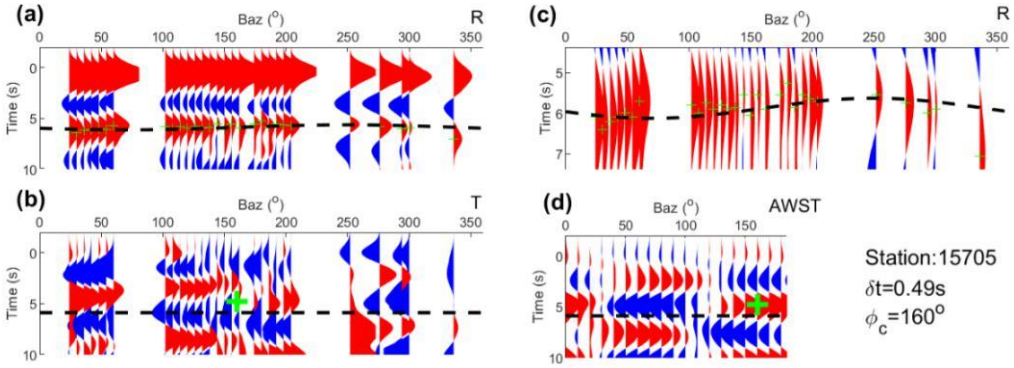

Figure 3. Same as **Figure 2** except for station 61075.

Figure 3 indicates the results of station 15705 representing a kind of station with 2π periodicity of arrivals of PMs against back-azimuth, which implies a single layer of anisotropy with a tilted symmetry axis. For the present study, there are 14 stations with a period rule of 2π, which are represented as a yellow triangle in Figure 1a. There are 201 RRFs and TRFs in the station 15705. We determined the delay time and the FD by fitting the arrivals of PMs with a periodicity of 2π caused by the anisotropic layer of inclined symmetry axis, as shown in Figure 3.

3. Results and discussions

3.1 Crustal anisotropy

Following the same data processing of Section 2, we obtained the anisotropic results for all the 92 stations. The results of all other stations are shown in Figure S1 and the parameters of crust anisotropy are listed in Table S1 and are provided as supplementary materials.Figure 4 indicates the distribution of crust anisotropy in the study area. The results indicate that the main FD of the anisotropic layer are N-S and NE-SW with delay times of 0.01 to 1.16s as shown by the red rose diagram in Figure 4. As the distribution of the FD has obvious local features, we divided the research area into 4 parts: Alax Block, north of Ordos, south of Ordos and Weihe

graben, and Yangtze Block (Figure 4).

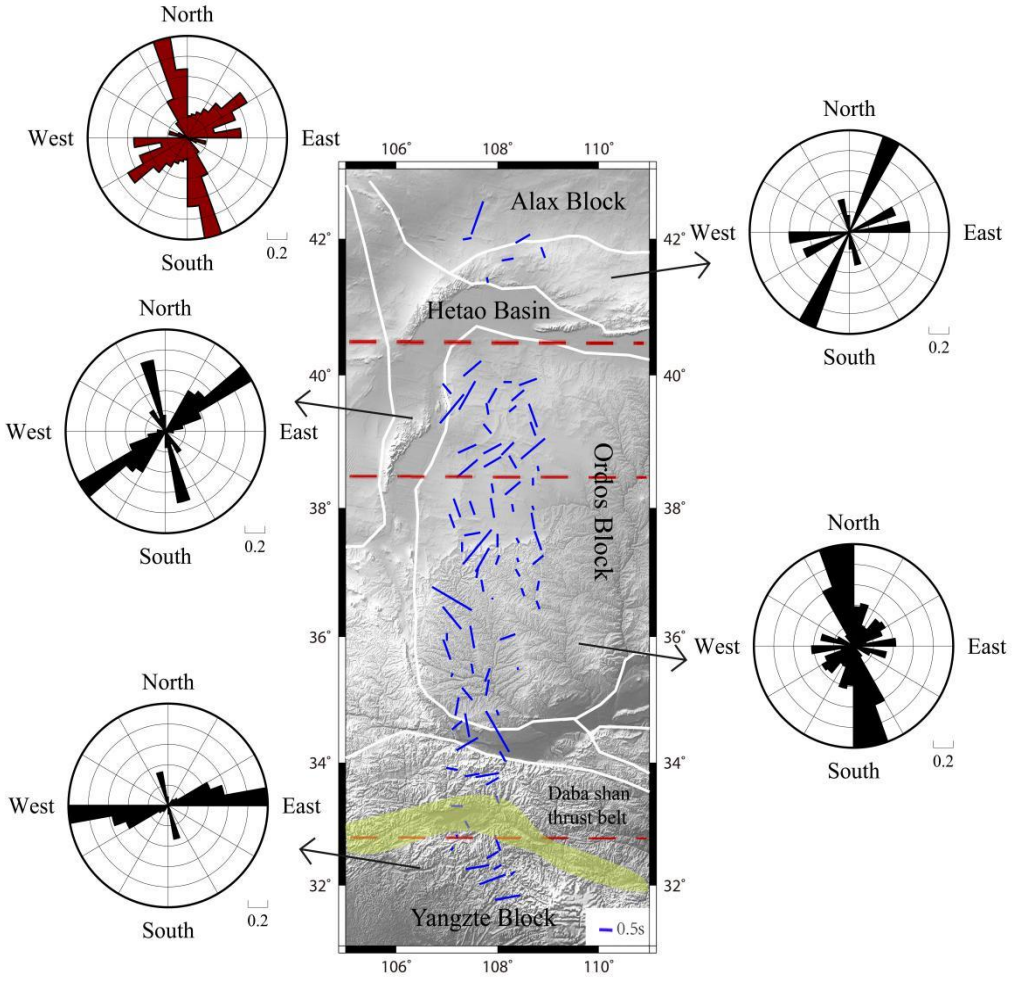

Figure 4. Map of anisotropy in the crust. White lines are the block boundary. DTB: Daba shan thrust belt. The yellow part is Daba shan thrust belt. The lengths of the blue line indicate the delay times, and their orientations are fast polarization directions. The rose diagrams correspond to the fast wave directions in a different region. The red rose diagram shows the results of all stations (Equal-area project rose diagram of the fast direction of all selected events).

In the Alxa block, the dominant direction of the fast wave is NEE-SSW with the delay time of 0.14 to 0.86s. In north Ordos block, the dominant direction of the fast wave is NEE-SWW with the delay time of 0.13 to 0.93s. In south Ordos block and the Weihe graben, the dominant direction of the fast wave is N-S with the delay time of 0.01 to 1.16s. In the Yangtze block, the dominant direction of the fast wave is E-W with the delay time of 0.09 to 0.64s.

The Cenozoic boundary of the Ordos block and the Yangtze block is not a boundary of crust anisotropy; however, the Dabashan fold-thrust belt in the Yangtze block is a boundary of crust anisotropy. The Dabashan fold-thrust belt is a key region in which the South China Block moved to the NW and was obliquely subducted under the North China block in Middle Triassic (Li et al., 2014). Therefore, the obvious differences in the crust anisotropy on either side of the Dabashan fold-thrust belt represent the difference of ancient crust of South China block and North China block. The results also indicate that the crust anisotropy can keep the information of the ancient time.

Both the Alxa and the Ordos block belonged to the North China block in the earlier geological time. The N-S fast direction of the anisotropic layer, therefore, might represent the crust characteristics of the ancient North China block. Also, the FD of the anisotropic layer in north Ordos block is obviously different from south Ordos and the Alxa block. In north Ordos block, the fast wave direction shifts from NNW- SSE to NEE- SWW from north to south, which might be caused by the upwelling of mantle material in mid-to-late Mesozoic era beneath the northern margin of the Ordos block as revealed by the three-dimensional (3D) MT inversion results (Dong et al., 2014). The upwelling of mantle material may have occurred in Hetao Basin and flowed southward into the interior of Ordos Block, resulting in the fossil anisotropy transformation of Ordos Block. The high Vp/Vs ratios constrained by receiver functions (Wang et al., 2017; Huang et al., 2020) also imply the presence of hot material in the lower crust.

Recently, more and more scholars have used receiver function to obtain anisotropy, mainly using the Moho Ps phase splitting to estimate bulk crustal anisotropy (Liu and Niu, 2012; Shen et al., 2015; Sun et al., 2015; Niu et al., 2016;Wirth et al., 2017;Bar et al., 2019). They developed an integrated technique for estimating crustal anisotropy and it's could be applied to any broadband seismic stations that have a good backazimuthal coverage of teleseismic events(Liu and Niu, 2012). Sun et al.(2015) estimated the crustal structure and deformation under the Longmenshan and its surroundings by analyzing receiver function data. But others argue that this approach to anisotropy is unreliable (Brownlee et al., 2017; Lamarque & Agostinetti, 2020). In the opinion of them, the actual situation of deep earth anisotropy is more complicated, and it is difficult to obtain several thousand meters of anisotropic layer by this method. In fact, we also agree that the anisotropic layers deep in the earth's crust do not exist alone. But we can still get

some distinct and meaningful features of local crust anisotropy by analyzing a large amount of receiver function data recorded by the dense broadband seismic array.

3.2 Comparison with the SKS/SKKS results

Based on the previous studies of the Ordos block and its adjacent areas, it is generally observed that the delay time of crustal contribution is smaller than that of the SKS/XKS acquisitions (Chang et al., 2011; Sherrington et al., 2004; Weeraratne et al., 2009). In addition, the lower mantle is considered to be isotropic (Savage et al., 1999). Therefore, it is generally believed that the anisotropy measured by the SKS splitting mainly represents the anisotropy of the upper mantle. Figure 5a displays the crust anisotropy of our results, and the SKS (SKKS) results (Chang et al., 2017).

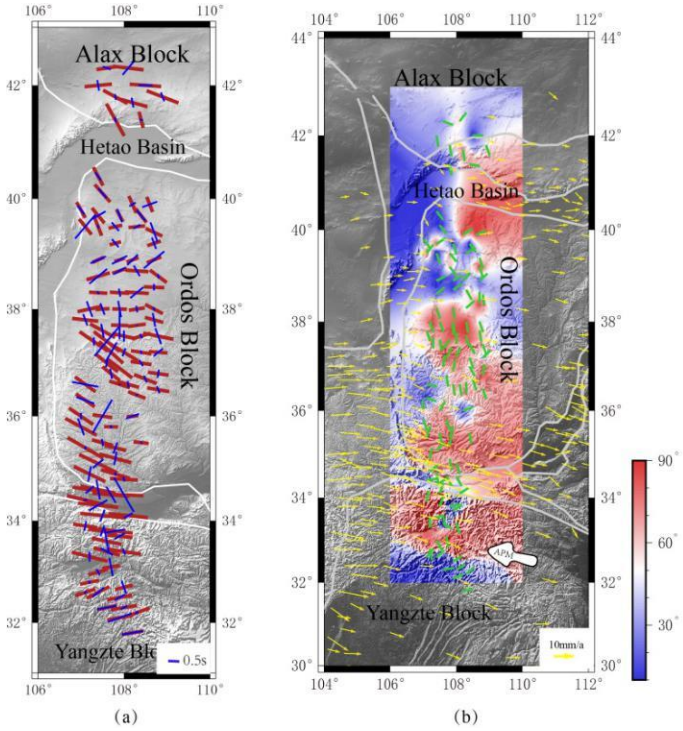

Figure 5. Results in comparison to the previous XKS results. (a) Gray line is the block dividing line. The rose diagram shows XKS results in different research areas. Red lines indicate XKS result (Chang et al., 2017). (b) The spatial distribution of the absolute value of the difference in the direction of rapid polarization between the crust and mantle. All the fast polarization directions of Figure 5a. According to this result, we can observe the coupling of crust and mantle in the Ordos. Yellow arrows indicate GPS results (Niu et al., 2005). Green lines indicate FD. A white arrow indicates an absolute plate motion (APM) direction.

Coupling and decoupling are the two typical interaction modes between the crust and the mantle. The anisotropy of the crust and the upper mantle is a good indicator of the coupling and decoupling mode. In order to display the visual anisotropy differences between them, we calculated the absolute values of differentials of the fast wave direction between the crust from receiver functions and the mantle from the SKS splitting (Figure 5b). If the absolute value is larger, the region is in a decoupled state; otherwise, it is in a coupled state. Certainly, this is a relative simple hypothesis, but it is still a little valuable to understand the crust and mantle movement under the current state of data resolution.

There is an obvious boundary of interaction mode between the crust and the mantle with the latitude of 38°. In north Ordos block with latitude larger than 38°, the crust and mantle are coupling, while the crust and mantle are decoupling in south Ordos block with latitude less than 38^{o}.

The E-W is the main direction of the upper mantle materials migration in south Ordos block, which might be caused by the Tibetan Plateau squeezing “out” eastward (Yu et al., 2016). The fast wave direction of crustal anisotropy and the upper mantle is totally different (Figure 5b), implying that the eastward mantle material has little influence on the structure of the crust, which still retains the stable structure of the ancient North China Craton.

The crust anisotropy in the north of the Ordos block is different from that in the south. The Crust-mantle coupling occurred to the north of 38°N of the Ordos block (ignoring the results of a few stations), while the strength of crustal anisotropy tended to increase (Figure 4). The delay time in the crust is obviously longer than other study areas; also, the upper mantle delay time is much shorter than other study areas. In the Yangtze block, the crust and upper mantle are coupled again, and the direction of the fast wave polarization is nearly parallel to the direction of the absolute plate movement (APM) of 104°NE (Kreemer et al., 2003), confirming the lithospheric crust-mantle coherent deformation model (Silver, 1996; Vinnik et al., 1992).

3.3 Integration with other seismic results

The Ordos block has been considered as a stable Archean Craton Block (An and Shi, 2006) with medium related to feldspar lithology in the lower crust (Liu et al., 2006). However, some recent results indicate that the crust of the Ordos block is not totally consistent with the typical

craton crust with a lower Vp/Vs ratio. For example, results from the receiver functions indicate that the thickness of the crust decreased significantly with the latitude larger than 38° (Huang et al., 2020). The northern part of the Ordos block is characterized by a larger velocity jump as well as a large Vp/Vs ratio (Figure 6), indicating that the crust beneath the station may be a mafic rock (Wang et al., 2017). Previous results (Dong et al., 2014; Guo et al., 2017; Tian et al., 2011) from tomography documented that the obvious low-velocity anomaly existed in the lower crust and the upper mantle from the north of Ordos block to the Hetao basin. It is speculated that an upwelling mantle material might exist under the north Ordos block. The upwelling mantle material has invaded the crust of the northern Ordos from north to south, caused the partial melt of the lower crust, Moho uplift, a higher Vp/Vs ratio, and a larger velocity jump of Moho. The fusion of mantle material and crustal material might also lead to a decrease in density jump, as mentioned by Huang et al. (2020). The distinct difference of the fast wave direction of the crust anisotropy in north Ordos block might also because of the immersion and modification of the upwelling mantle.

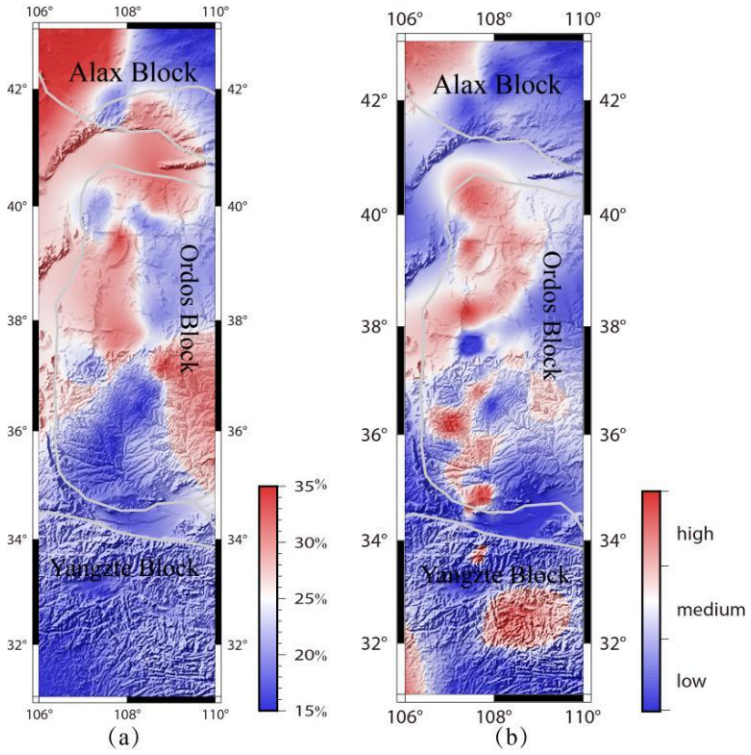

Figure 6. Results of the study area. (a) Results of velocity contrast from crust (Huang et al., 2020). (b) Results of the crustal Vp/Vs ratio (Wang et al., 2017).

Based on the previous results and the results of the crust anisotropy, we present a simplified sketch of the geodynamic model in the west Ordos block and its adjacent regions (Figure 7). The Dabashan fold-thrust belt is a contrasting boundary of crust anisotropy beneath ancient South China block and North China block. Another prominent feature of the model is the upwelling of mantle material in north Ordos block and the horizontal flow of mantle material in south Ordos block. Especially, the upwelling mantle material led to the partial melt of the lower crust, Moho uplift, the decrease of density jump, and the distinct difference of the fast wave direction of crust anisotropy in north Ordos block.

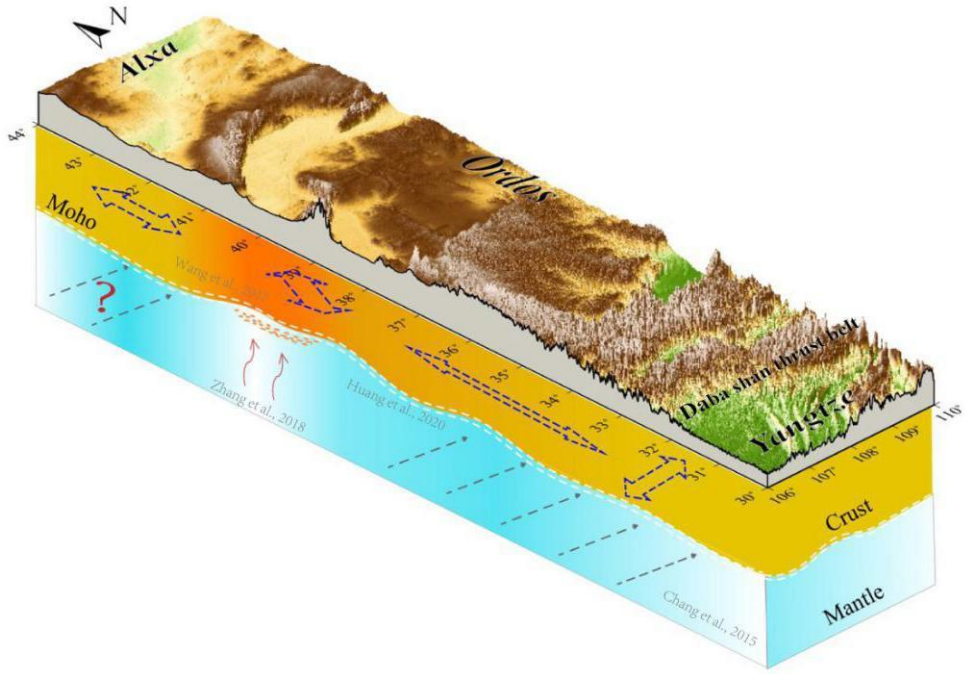

Figure 7. Crust-mantle interaction model. The orange part represents the crustal model, and the deeper color represents the high results of the crustal velocity ratio. (Wang et al., 2017). The blue part represents the mantle model, and the lighter color represents a smaller density jump (Huang et al.,2020). The white double dashed line represents the boundary between the crust and the mantle. Blue dashed arrow indicates the FD of the crust. Grey dashed line represents the squeeze from the Tibetan Plateau. The red arrow indicates the upwelling of hot materials (Zhang et al., 2018).

Combined with the results of previous studies(Huang et al., 2020; Dong et al., 2014; Guo et al., 2017; Chang et al., 2017), we believe that the partial melting in the north of Ordos block

might be caused by thermal erosion, resulting in slow crust subsidence. It is also a sign that the north of the Ordos block may be experiencing very slow craton destruction.

4. Conclusions

Based on the numerous observations from the 92 broadband seismic stations of Chin Array-Himalaya II seismic array in the Ordos block, we determined the crust anisotropic parameters of the block and its adjacent areas using radial and tangential receiver functions.

By analyzing the relationships between the results of the SKS splitting and the receiver functions, we discussed the interaction mode between the crust and mantle. As compared to the other regions, the results of anisotropic parameters in the north of Ordos are different. In the north Ordos block, the crust and mantle are coupling as represented by the consistent fast direction of the SKS splitting and the receiver functions. In the south Ordos block, the crust and mantle are decoupling and are represented by the nearly perpendicular fast direction of the SKS splitting and the receiver functions.

Combining the results of tomography, crustal velocity ratio, crustal thickness, and Moho features, we observed the contrasting structures beneath north and south Ordos block. The obvious low-velocity abnormalities, larger velocity ratios, and a distinct Moho velocity jump indicate the partial melting in the upper mantle in north Ordos block, which implies the upwelling of mantle material. Based on this, we deduced that the north Ordos block might be currently experiencing craton destruction. The remarkable differences of velocity structures in north and south Ordos block is mainly attributed to the different movement of mantle material.

Acknowledgements: We acknowledge the National Key Research and Development Program of China (2017YFC1500100), National Natural Science Foundation of China (Grant 41874052 and 41730212), the Second Tibetan Plateau Scientific Expedition and Research Program (STEP) (2019QZKK0701, 2019QZKK0901), Guangdong Province Introduced Innovative R&D Team of Geological Processes and Natural Disasters around the South China Sea (2016ZT06N331). Some figures were plotted with Generic Mapping Tools (Wessel & Smith, 1995).

References

An, M., & Y, Shi (2006), Lithospheric thickness of the chinese continent, Physics of the Earth & Planetary Interiors, 159(3-4), 0-266. https://doi.org/10.1016/j.pepi.2006.08.002.

Bar, N., M. D. Long, L. S. Wagner, S. L. Beck, G. Zandt, & H. Tavera (2019), Receiver function analysis reveals layered anisotropy in the crust and upper mantle beneath southern peru and northern bolivia, Tectonophysics, 753, 93-110, doi:10.1016/j.tecto.2019.01.007.

Brownlee, S.J., V. Schulte-Pelkum, A. Raju, K. Mahan, C. Condit, and O.F. Orlandini (2017), Characteristics of deep crustal seismic anisotropy from a compilation of rock elasticity tensors and their expression in receiver functions, Tectonics, 36, 1835– 1857, doi:10.1002/2017TC004625.

Chang, L.J., C.Y. Wang, Z.F. Ding (2011), Upper mantle anisotropy in the Ordos block and its margins, Sci. China Earth Sci., 54: 888–900. https://doi.org/10.1007/s11430-010-4137-2.

Chang, L.J., Z.F. Ding, C.Y. Wang, L.M. Flesch (2017), Vertical coherence of deformation in lithosphere in the NE margin of the Tibetan plateau using GPS and shear-wave splitting data, Tectonophysics, Volume 699, Pages 93-101, ISSN 0040-195. https://doi.org/10.1016/j.tecto.2017.01.025.

Crampin, & Stuart (1987), Geologic0al and industrial implications of extensive-dilatancy anisotropy., Nature, 328(6130), 491-496. https://doi.org/10.1038/328491a0.

Deng, J.F., X.X. Mo, H.L. Zhao, Z.X. Wu, Z.H. Luo, S.G. Su (2004), A new model for the dynamic evolution of Chinese lithosphere: 'continental roots-plume tectonics', Earth Sci. Rev., 65, pp. 223-275. https://doi.org/10.1016/j.earscirev.2003.08.001.

Deng, Q.D., S.P. Cheng, W. Min, G.Z. Yang, D.W. Reng (1999), Discussion on Cenozoic tectonics and dyamics of Ordos block, Journal of Geomechanics (in Chinese), 5(3):13-21.

Ding, G.Y. (1991), Lithospheric Dynamics of China (in Chinese), Beijing: Seismological Press.

Dong, H., W.B. Wei, G.F. Ye, S. Jin, A.G. Jones, J.N. Jing, L.T. Zhang, C.L. Xie, F. Zhang, H. Wang (2014), Three-dimensional electrical structure of the crust and upper mantle in Ordos block and adjacent area: Evidence of regional lithospheric modification. Geochem. Geophy, Geosyst. 15(6). https://doi.org/10.1002/2014GC005270.

Dong, Y.P., M. Santosh (2016), Tectonic architecture and multiple orogeny of the Qinling Orogenic Belt, Central China. Gondwana Research 29, 1-40.

Frederiksen, A.W., M.G. Bostock (2010), Modelling teleseismic waves in dipping anisotropic structures,

Geophysical Journal of the Royal Astronomical Society, 141(2):401-412.

Gan, W., P. Zhang, Z.K. Shen, Z. Niu, M. Wang, Y. Wan, D. Zhou, J. Cheng (2007), Present-day crustal motion within the Tibetan Plateau inferred from GPS measurements, J. Geophys. Res. 112, B08416. https://doi.org/10.1029/2005JB004120.

Girardin, N., and V. Farra (1998), Azimuthal anisotropy in the upper mantle from observations of P-to-S converted phases: Application to southeast Australia, Geophys. J. Int., 133(3), 615–629.

Griffin, W.L., Z. Andi, S.Y. O'Reilly, & C.G. Ryan (1998), Phanerozoic evolution of the lithosphere beneath the Sino-Korean Craton, Mantle Dynamics and Plate Interactions in East Asia. American Geophysical Union (AGU).

Guo, B., Q.Y. Liu, J.H. Chen, D.P. Zhao, S.C. li, Y.G. Lai (2004), Seismic tomographic imaging of the crust and upper mantle beneath the Northeastern edge of the Qinghai-Xizang plateau and the Ordos area, Chinese J. Geophys. (in Chinese), 47(5):790～797. https://doi.org/10.1002/cjg2.566.

Guo, H.L., Z.F. Ding, X.M. Xu (2017), Upper mantle structure beneath the northern South-Nouth Seismic Zone from teleseismic traveltime data, Chinese J. Geophys. (in Chinese), 60(1):86-97. https://doi.org/10.6038/cjg20170108.

Huang, L.T., X. Shen, W.J. Zheng, Y.P. Qian, D.L. Zhang, W.T. Wang, X.L. Ii (2020), Moho properties of western Ordos block and surrounding regions constrained by teleseismic receiver functions and its tectonic implication, Chinese J. Geophys. (in Chinese) ,63 (3). https://doi.org/10.6038/cjg2020N0210.

Huang, Z., M. Xu, L.Wang, N. Mi, D. Yu, H. Li (2008), Shear wave splitting in the southern margin of the Ordos block, north China, Geophysical Research.Letters,35(19). https://doi.org/10.1029/2008gl035188.

Jia, M., X.G. Wang, Sh.L. Li, Y.S. Chen (2015), Crustals tructures of Ordos block and surrounding regions from receiver functions, Progress in Geophysics (in Chinese), 30(6):2474-2481. https://doi.org/10.6038/pg20150605.

Jia, S.X., F.Y. Wang, X.F. Tian, Y.H. Duan, J.S. Zhang, B.F. Liu, J.Y. Lin (2014), Crustal structure and tectonic study of North China Craton from a long deep seismic sounding profile, Tectonophysics, 627:48-56. https://doi.org/10.1016/j.tecto.2014.04.013.

Jie, X. (2001), Newly generated seismotectonic zones in North China and its regional seismotectonic framework. Scientia Geologica Sinica, 10(3), 9-18.

Kreemer, C., W.E. Holt, A.J. Haines (2003), An integrated global model of present-day plate motions and plate boundary deformation, Geophys. J. Int., 154, 8–34. https://doi.org/10.1046/j.1365-246X.2003.01917.x.

406 Lamarque, G., & N.P. Agostinetti (2020), Modeling of anisotropy in the lithosphere and asthenosphere for real Earth
407 cases: A critical assessment of the impact on SKS measurements, Journal of Geophysical Research: Solid Earth,
408 125. https://doi.org/10.1029/2019JB018978

409 Li, S.L., X.K. Zhang, C.K. Zhang, J.R. Zhao, S.X. Cheng (2002), A preliminary study on the crustal velocity
410 structure of Maqin–Lanzhou–Jingbian by means of deep seismic sounding profile, Chin. J. Geophys. 45, 210–
411 217.

412 Li, W.P., Sh.F. Liu, Q. Tao, G.X. Dou, T.J. Gao (2014), Analysis of structural deformation in the North Dabashan
413 thrust belt, South Qinling, central China, International Geology Review.
414 http://dx.doi.org/10.1080/00206814.2014.935966.

415 Ligorria, J.P., C.J. Ammon (1999), Iterative deconvolution and receiver-function estimation, Bulletin of the
416 Seismological Society of America, 89(5):1395-1400.

417 Liu, C.Y., H.G. Zhao, X.J. Gui, L.P. Yue, J.F. Zhao, J.Q. Wang (2006), Space-time coordinate of the evolution and
418 reformation and mineralization response in Ordos Basin, Acta Geol. Sin. 80, 617–638.

419 Liu, H., and F. Niu (2012), Estimating crustal seismic anisotropy with a joint analysis of radial and transverse
420 receiver function data, Geophys. J. Int., 188, 144–164.

421 Long, M.D. (2013), Constraints on subduction geodynamics from seismic anisotropy, Reviews of Geophysics, 51,
422 76-112.

423 Long, M.D., P.G. Silver (2009), Shear Wave Splitting and Mantle Anisotropy: Measurements, Interpretations, and
424 New Directions, Surv Geophys 30, 407-461. https://doi.org/10.1007/s10712-009-9075-1

425 Mccormack, K., E.A. Wirth, M.D. Long (2013), B-type olivine fabric and mantle wedge serpentinization beneath
426 the Ryukyu arc, Geophysical Research Letters, 40(9):1697-1702.

427 Niu, X., D. Zhao, J. Li, and A. Ruan (2016), P wave azimuthal and radial anisotropy of the Hokkaido subduction
428 zone, J. Geophys. Res. Solid Earth, 121, 2636–2660, doi:10.1002/2015JB012651.

429 Niu, Z.J., M. Wang, H. Sun (2005), Contemporary velocity field of crustal movement of Chinese mainland from
430 global positioning system measurements. Chin. Sci. Bull. 50 (9),939–941. http://dx.doi.org/10.1360/982005-
431 220

432 Savage, M.K (1999), Seismic anisotropy and mantle deformation: what have we learned from shear wave splitting?
433 Rev. Geophys. 37 (1), 65–106. http://dx.doi.org/10.1029/98RG02075.

Shen, X.Z., X.H. Yuan, and J.S. Ren (2015), Anisotropic low-velocity lower crust beneath the northeastern margin of Tibetan Plateau: Evidence for crustal channel flow, Geochem. Geophy. Geosyst., 16.12:n/a-n/a. https://doi.org/10.1002/2015GC005952.

Sherrington, H.F., G. Zandt, A.W. Frederiksen (2004), Crustal fabric in the Tibetan Plateau based on waveform inversions for seismic anisotropy parameters, J. Geophys. Res., 109 , Article B02312. https://doi.org/10.1029/2002JB002345.

Silver, P.G. (1996), Seismic anisotropy beneath the continents: probing the depths of geology. Annual Review of Earth & Planetary Sciences, 24(1), 385-432.

Silver, P.G., & W.W. Chan (1991), Shear wave splitting and subcontinental mantle deformation, Journal of Geophysical Research Solid Earth, 96(B10), 16429-16454. https://doi.org/10.1029/91jb00899.

Sun, Y., J. Liu, K. Zhou, B. Chen, and R. Guo (2015), Crustal structure and deformation under the Longmenshan and its surroundings revealed by receiver function data, Phys. Earth Planet. Inter., 244, 11–22.

Tian, X.B., J.W. Teng, H.S. Zhang, Z.J. Zhang, Y.Q. Zhang, H. Yang, K. Zhang (2011), Structure of crust and upper mantle beneath the Ordos block and the Yinshan Mountains revealed by receiver function analysis. Physics of the Earth & Planetary Interiors, 184(3):186-193. https://doi.org/10.1016/j.pepi.2010.11.007.

Vinnik, L.P., L.I. Makeyeva, A. Milev, A.Y. Usenko (1992), Global patterns of azimuthal anisotropy and deformations in the continental mantle, Geophys. J. Int., 111 (3), pp. 433-447. https://doi.org/10.1111/j.1365-246X.1992.tb02102.x.

Wang, W.L., J.P. Wu, L.H. Fang, G.J. Lai, Y. Cai (2017), Sedimentary and crustal thicknesses and Poisson's ratios for the NE Tibetan Plateau and its adjacent regions based on dense seismic arrays, Earth Planet. Sci. Lett. 462:76-85. http://dx.doi.org/10.1016/j.epsl.2016.12.040.

Weeraratne, D.S., S. Karalliyadda, P.G. Silver (2009), Very Little Crustal Anisotropy in Eastern Tibet from Regional S phases, the Game's Over, Eos. Trans. AGU. Fall Meet. Suppl. Abstract S11A-1690. https://ui.adsabs.harvard.edu/abs/2009AGUFM.S11A1690W.

Wessel, P., W.H.F. Smith (1995), New version of the generic mapping tools, Eos, Transactions American Geophysical Union, 76(33):329-329. http://dx.doi.org/10.1029/95EO00198

Wirth, E. A., M.D. Long, J.C. Moriarty (2017), A Markov chain Monte Carlo with Gibbs sampling approach to anisotropic receiver function forward modeling, Geophysical Journal International, Volume 208, Issue 1, Pages 10–23. https://doi.org/10.1093/gji/ggw383

463 Yu, Y., Y.J. Chen (2016), Seismic anisotropy beneath the southern Ordos block and the Qinling-Dabie orogen,
464 China: Eastward Tibetan asthenospheric flow around the southern Ordos, Earth Planet. Sci. Lett. 455:1-6.
465 http://dx.doi.org/10.1016/j.epsl.2016.08.026.

466 Zhang, F., Q. Wu, Y. Li (2018), Seismic Tomography of Eastern Tibet: Implications for the Tibetan Plateau Growth,
467 Tectonics, 37(9-10): 2833- 2847. http://dx.doi.org/10.1029/2018TC004977

Figure 1.

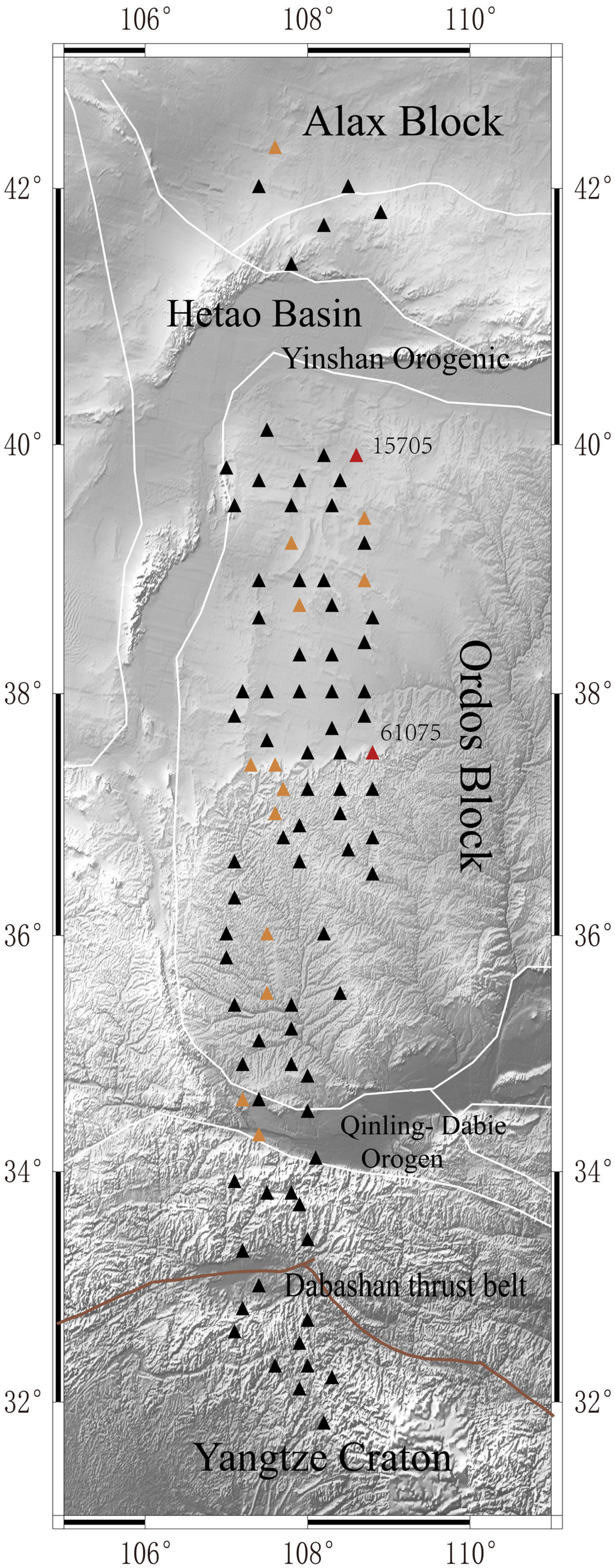
106°
108°
110°
42°
40°
38°
36°
34°
32°
Alax Block
Hetao Basin
Yinshan Orogenic
15705
61075
Ordos Block
Qinling- Dabie
Orogen
Dabashan thrust belt
Yangtze Craton

(a)

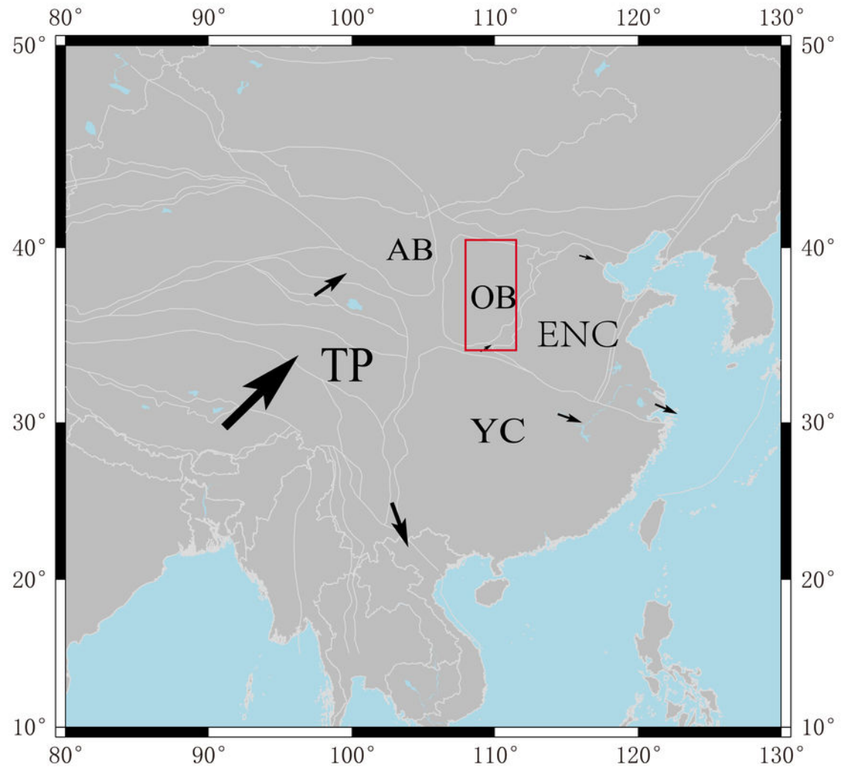
80°
90°
100°
110°
120°
130°
50°
40°
30°
20°
10°
AB
OB
ENC
TP
YC

(b)

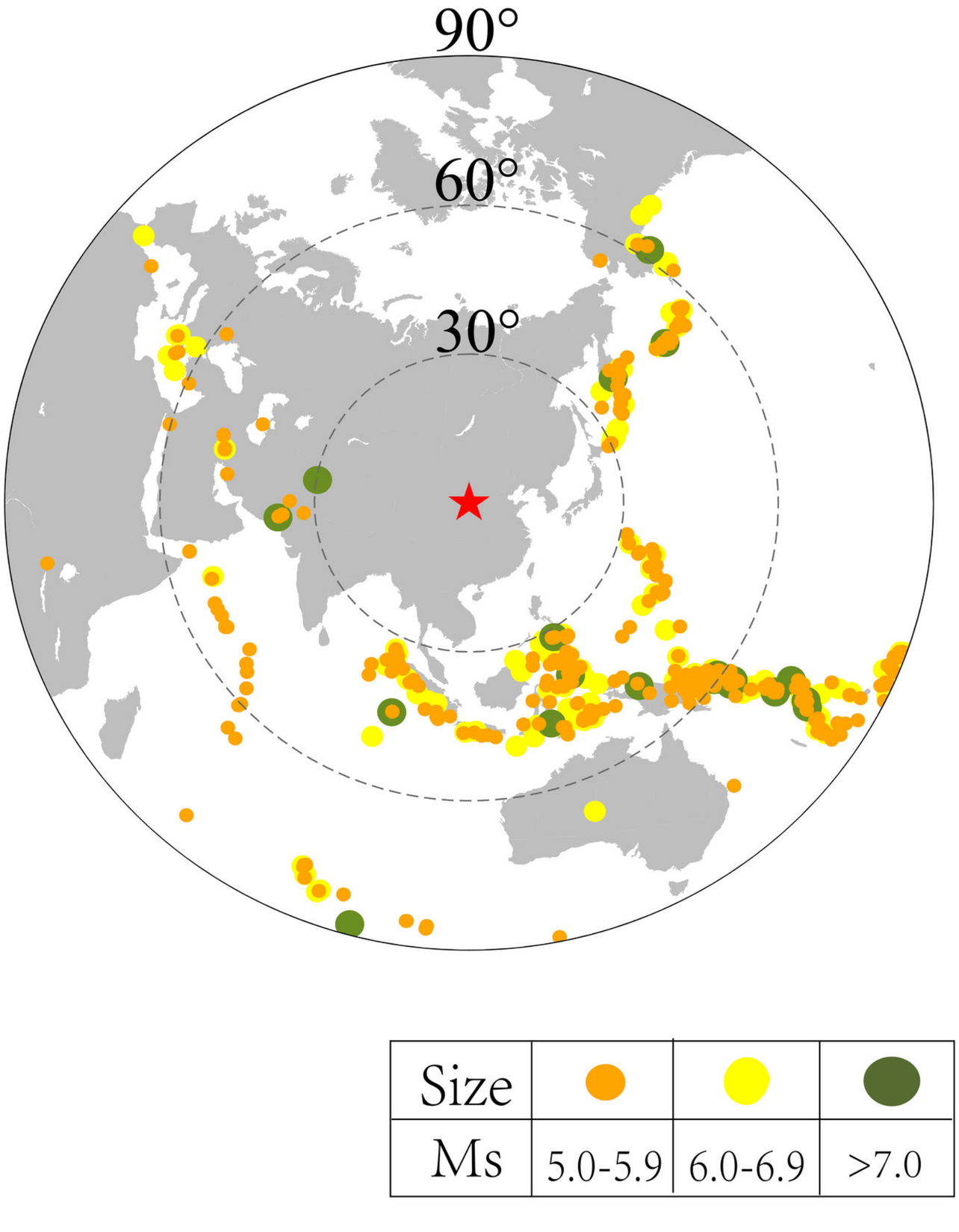
90°
60°
30°
Size
Ms
5.0-5.9
6.0-6.9
>7.0

(c)

Figure 2.

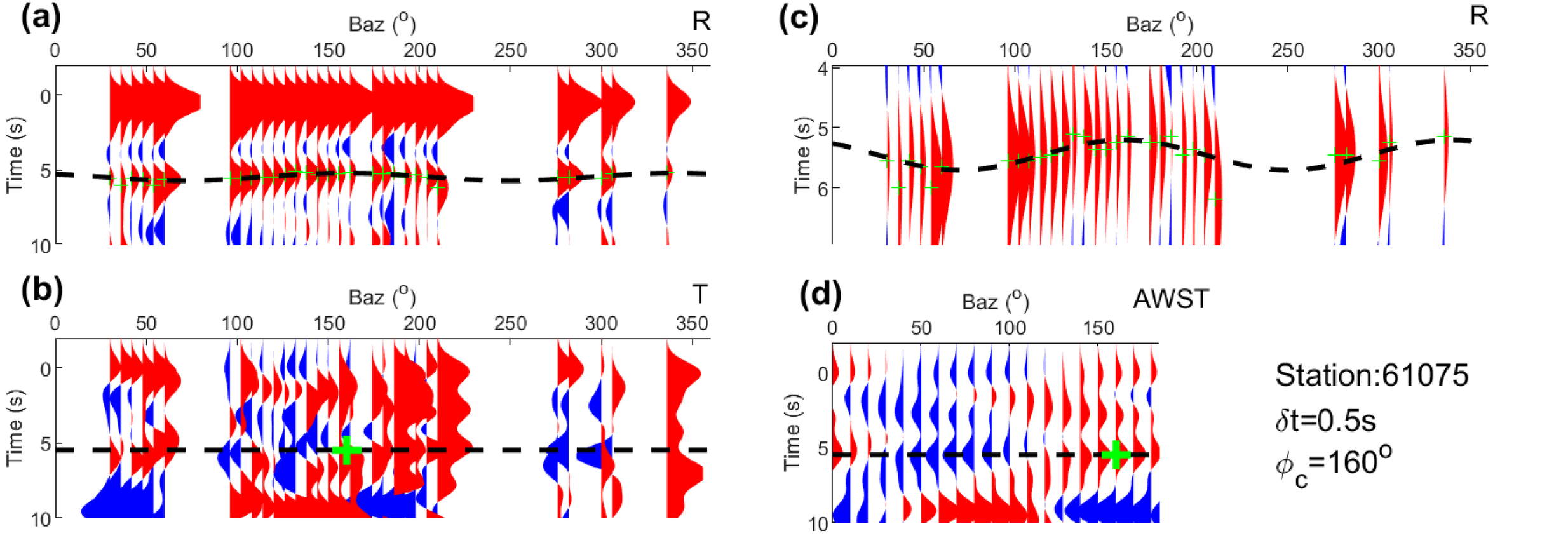
(a)
Baz (°)
R
Time (s)
(b)
T
(c)
(d)
AWST
Station:61075
δt=0.5s
ϕ_c=160°

Figure 3.

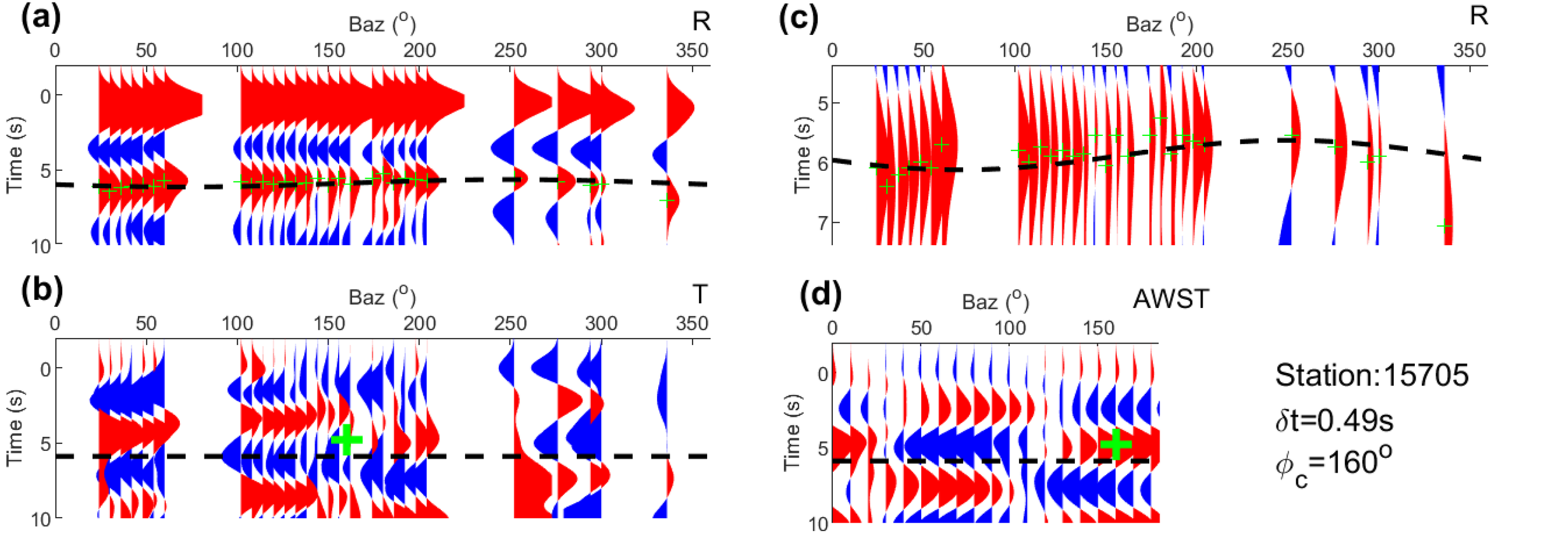
(a)
Baz (°)
R
0
50
100
150
200
250
300
350
Time (s)
0
5
10
(b)
Baz (°)
T
0
50
100
150
200
250
300
350
Time (s)
0
5
10
(c)
Baz (°)
R
0
50
100
150
200
250
300
350
Time (s)
5
6
7
(d)
Baz (°)
AWST
0
50
100
150
Time (s)
0
5
10
Station:15705
δt=0.49s
ϕ_c=160°

Figure 4.

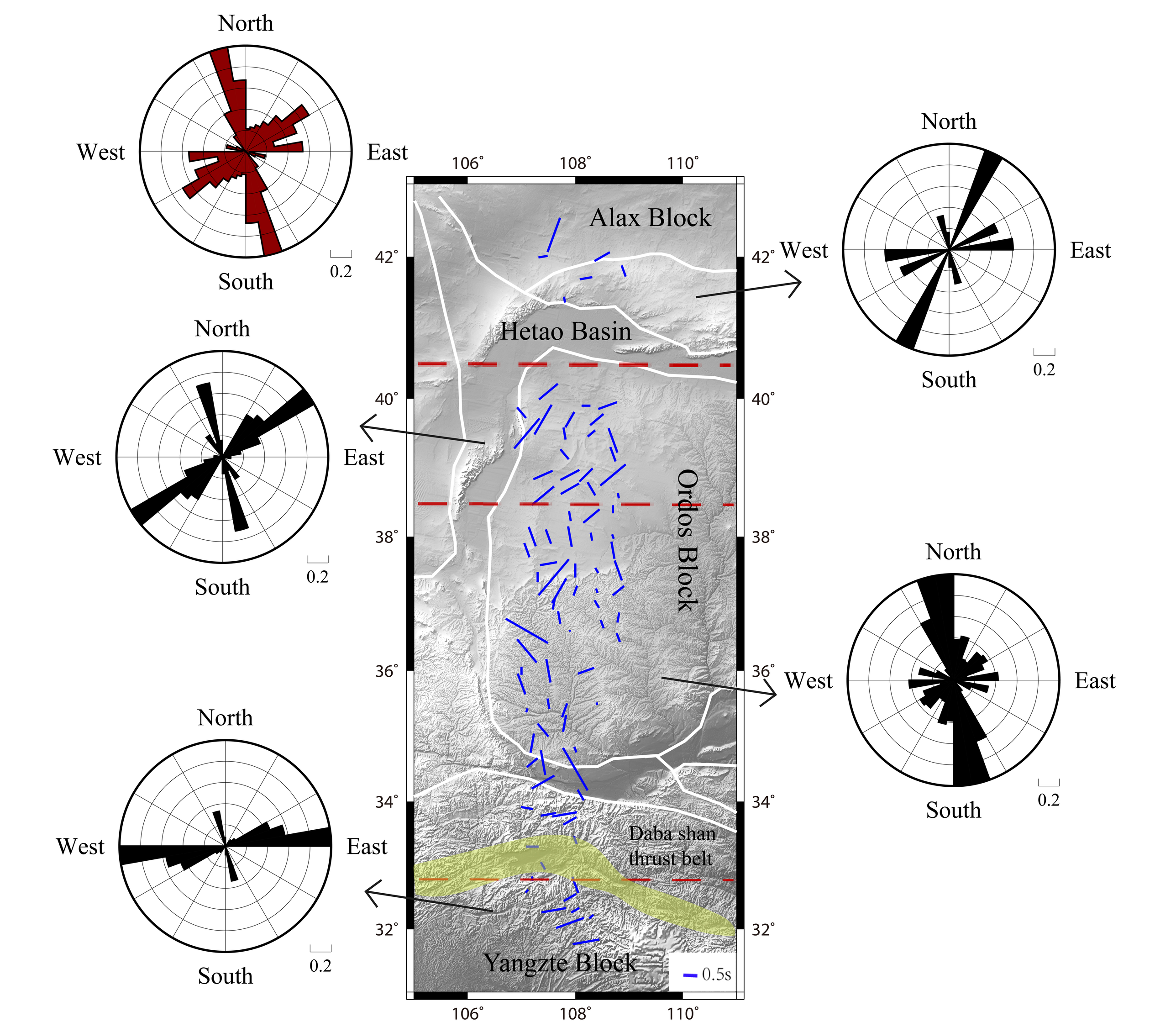
North
West
East
South
0.2
106°
108°
110°
42°
40°
38°
36°
34°
32°
Alax Block
Hetao Basin
Ordos Block
Daba shan
thrust belt
Yangzte Block
0.5s

Figure 5.

106°
108°
110°
42°
40°
38°
36°
34°
32°
Alax Block
Hetao Basin
Ordos Block
Dabashan
thrust belt
Yangzte Block
(a)
104°
106°
108°
110°
112°
44°
42°
40°
38°
36°
34°
32°
30°
Alax Block
Hetao Basin
Ordos Block
Dabashan
thrust belt
Yangzte Block
10mm/a
90°
60°
30°
(b)

Figure 6.

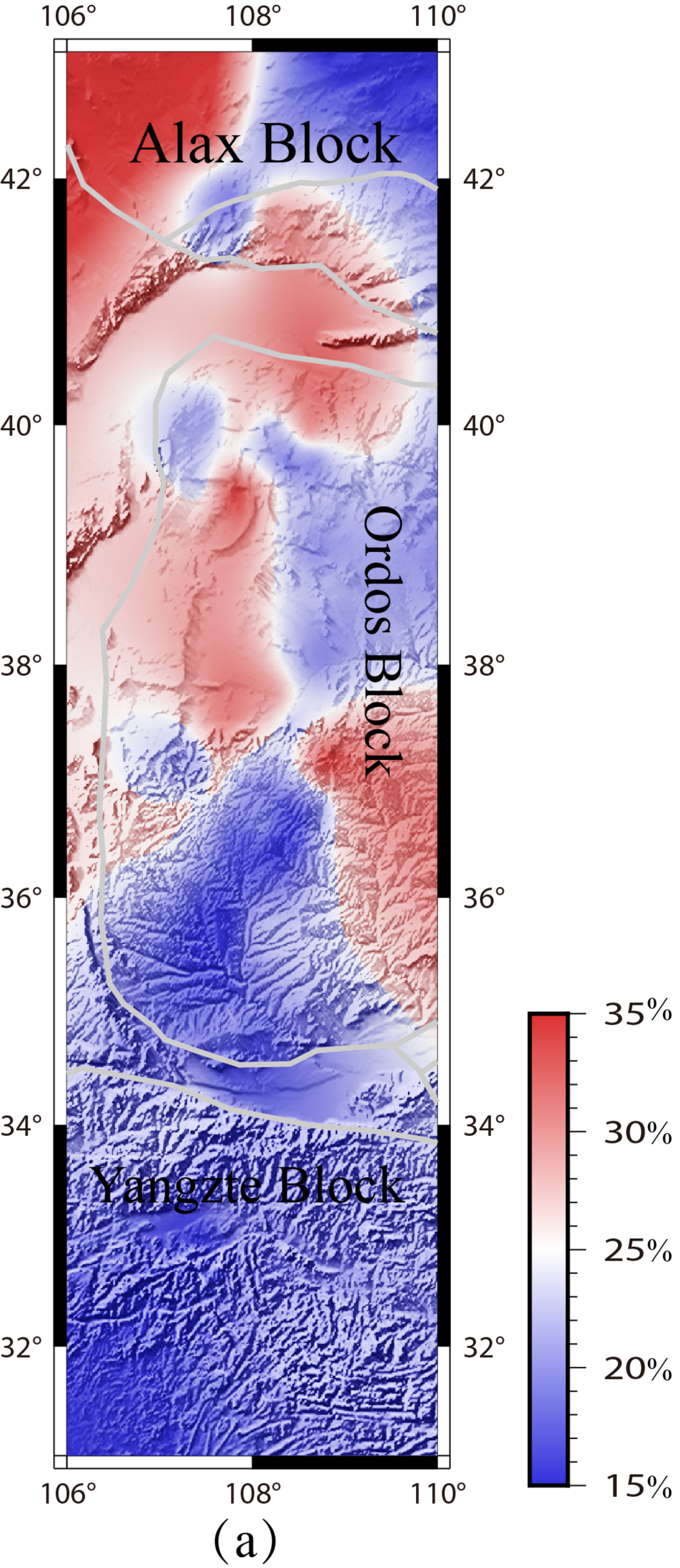
106°
108°
110°
42°
40°
38°
36°
34°
32°
Alax Block
Ordos Block
Yangzte Block
35%
30%
25%
20%
15%

(a)

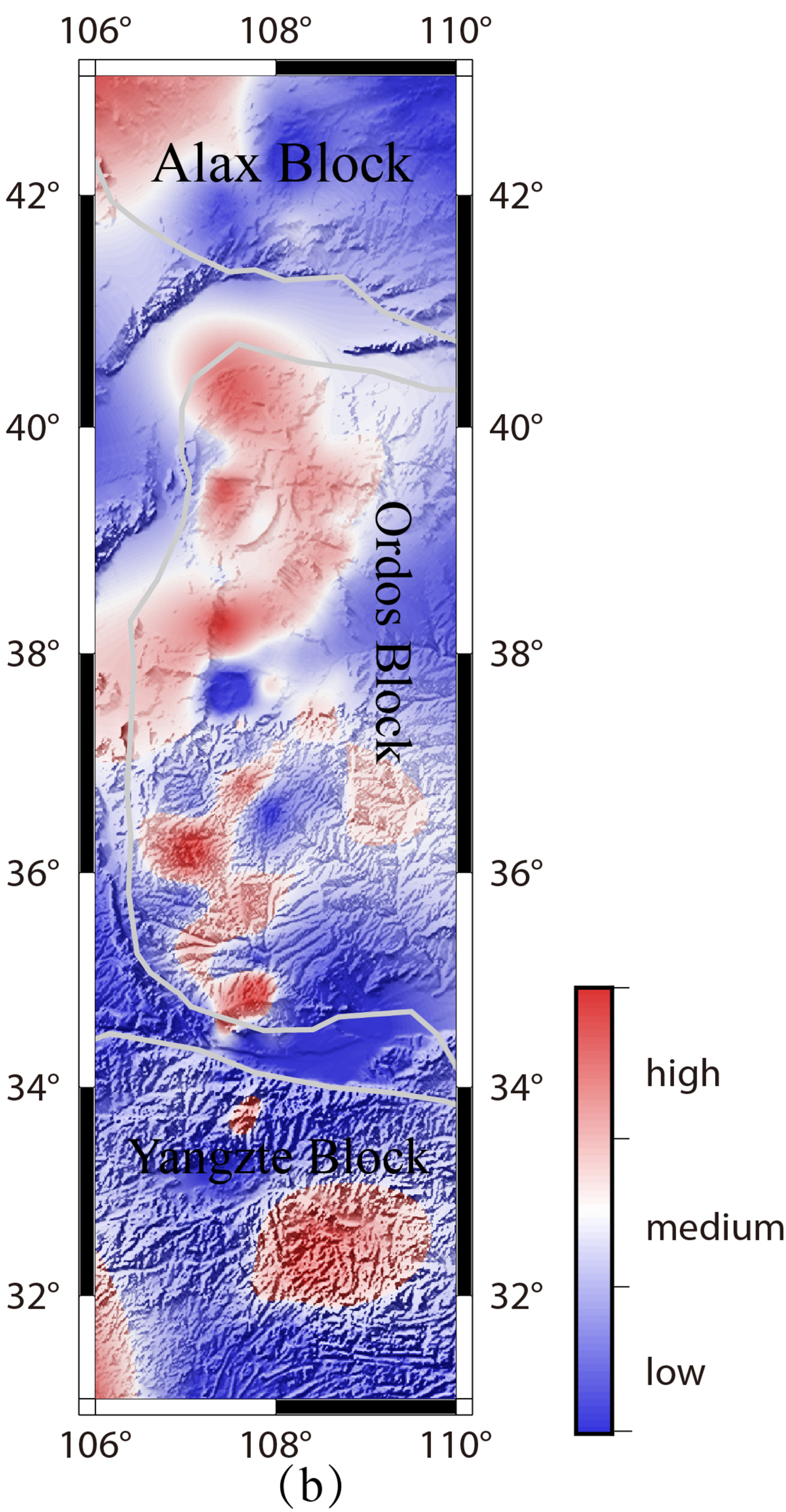
106°
108°
110°
42°
40°
38°
36°
34°
32°
Alax Block
Ordos Block
Yangzte Block
high
medium
low

(b)

Figure 7.

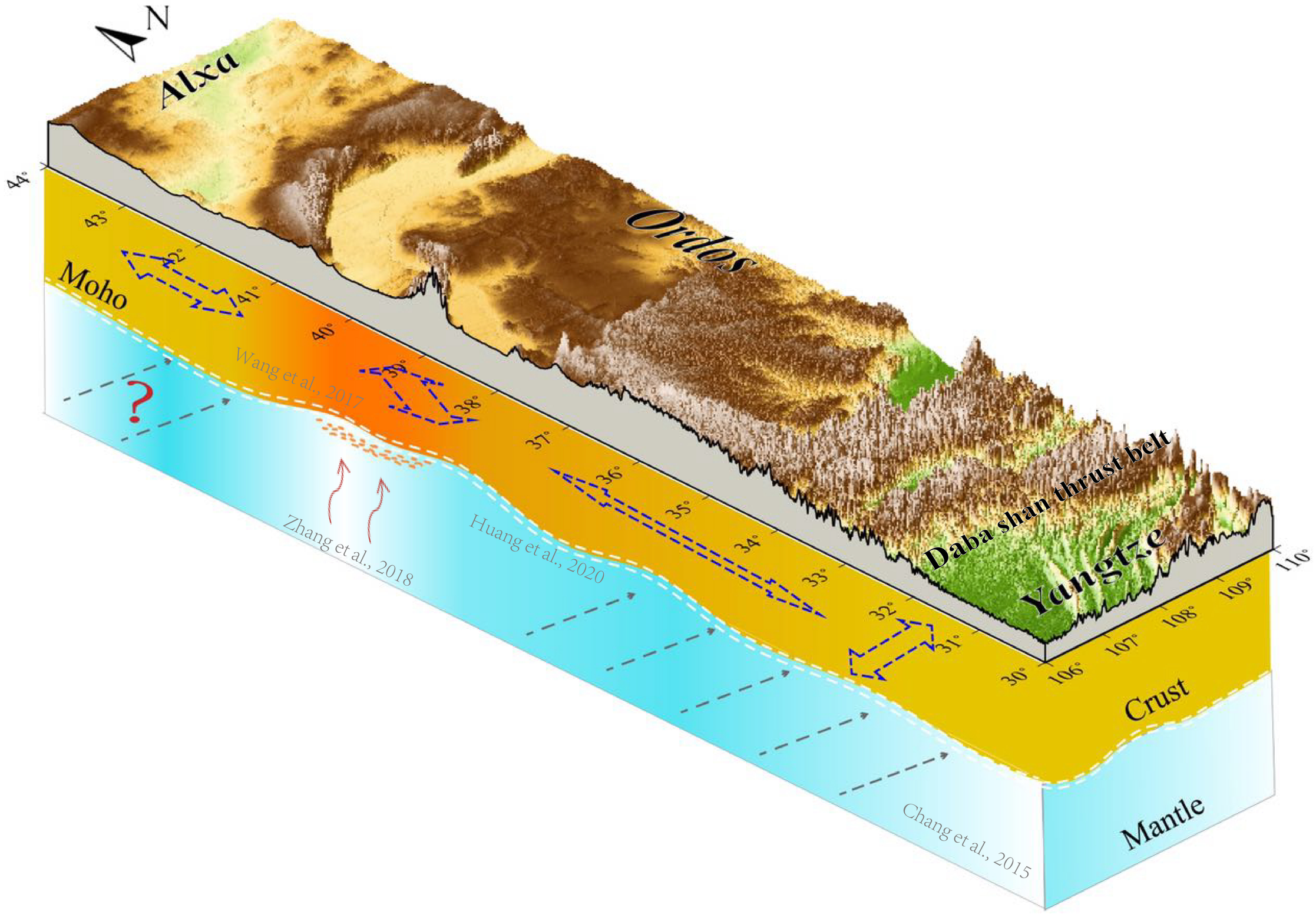
N
Alxa
Ordos
Daba shan thrust belt
Yangtze
Moho
Crust
Mantle
?
Wang et al., 2017
Zhang et al., 2018
Huang et al., 2020
Chang et al., 2015
44°
43°
42°
41°
40°
39°
38°
37°
36°
35°
34°
33°
32°
31°
30°
106°
107°
108°
109°
110°